



Improvement of electrical and mechanical properties of laser welded lap joints via dimensional optimization

Gábor Horváth¹ · Andor Körmöczy¹ · Tamás Szörényi¹ · Zsolt Geretovszky¹

Received: 19 July 2023 / Accepted: 29 November 2023 / Published online: 14 December 2023
© The Author(s) 2023

Abstract

With the proliferation of electric drivetrains, the development and optimization of joining techniques for the fabrication of battery packs became a prime manufacturing topic. Decreasing the electrical resistance and increasing the mechanical strength of the welds at the individual cell level are of great importance not only for productivity and efficiency but also for safety and sustainability purposes. Lasers offer an advanced, highly automatable solution for battery cell joining. Usually, the optimization focuses on the laser parameters or the scanning speed. However, the most widespread battery welding geometry, the so-called lap geometry, allows alternative possibilities for joint property optimization. The novelty of our approach is that we focus on systematic experimental investigation of the effects of dimensional parameters and the layout of the weld pattern. Systematic experiments reveal that the shape and size of the weld area have substantial effect on the properties of the laser welded joint. Our results prove that a rather substantial gain can be achieved in both the electrical and mechanical properties when the weld consists of at least two parallel bead segments. We also show that it is beneficial by both means if the segments have the greatest individual length and placed apart at the maximum feasible distance. The orientation of the straight segments affects the mechanical and electrical behavior differently: strongest welds consist of weld segments oriented in parallel, while the smallest resistance can be achieved using segments oriented perpendicular to the direction of current flow, respectively.

Keywords Laser lap welding · Electrical properties · Mechanical properties · Dimensional parameters

Nomenclature

U_{joint}	Joint voltage (V)
U_{base}	Base voltage (V)
ℓ_m	Measurement length (m)
$\ell_{overlap}$	Overlap length (m)
x	Sheet thickness (m)
I	Electric current (A)
R_{joint}	Electrical resistance of the joint (Ω)
R_{base}	Electrical resistance of the base (Ω)
A	Weld area (m^2)
TSS	Tensile shear strength (Pa)
E	Extent (m)
N	Number of segments
s	Segment spacing (m)
L	Segment length (m)

1 Introduction

When producing battery packs for electrical vehicles or other electrically powered machines, a substantial amount of small electrical sources must be conjoined. This stems from the large power need of the electrical consumers and the limited capacity of individual batteries [1]. For the joining process several joining techniques are suitable, but for each and every one of them a thorough optimization process must be carried out to perfect the given bonding process on the lowest assembly levels. As a result, a substantial improvement can be ultimately achieved either in terms of electrical resistance, mechanical strength, weight, battery life, and so on, depending on the aims of the optimization process.

In general, among the numerous welding techniques laser welding is considered to be one of, if not the best solution for battery joining applications. It is highly automatable, works with very low heat input and small heat affected zone sizes and exhibits excellent reproducibility [2, 3]. The most common and widely discussed properties of laser welded joints are the mechanical strength of the bonds [4–7] and

✉ Zsolt Geretovszky
gero@physx.u-szeged.hu

¹ Department of Optics and Quantum Electronics, University of Szeged, Dóm tér 9., 6720 Szeged, Hungary

recently with the appearance of electrical vehicles the electrical resistance of the joints [8, 9]. The mechanical and electrical parameters are in most cases optimized independently, and most frequently via varying the laser process parameters such as incident laser power, scanning speed, beam diameter, and incidence angle [10]. To further support this, we note that more recent papers also focus on implementing numerical calculations and conducting experiments regarding the changes occurring in the depth and width of the melt pool induced by the alteration of laser process parameters [11, 12]. Even the most up-to-date publications of laser welding optimization, the AI-assisted analysis and property prediction of laser welded joints, are primarily focusing on acquiring an optimized set of laser parameters and conditions using deep learning methods [13–15]. However, the lap joint configuration offers several other parameters (other than laser process parameters) that contribute to the final resistance and strength of the joint, thus providing further room for optimization [16–18].

For battery laser welding the lap joint configuration is widely used both in direct battery to busbar and wire/ribbon bonding configurations [19–21]. Most of these lap joints are manufactured with a laser welding setup equipped with a scanner optic that is ideally suited for the optimization of the dimensional parameters of the weld, as well.

Along these lines several groups have already made attempts to study and model the behaviors and optimize the properties of the laser welded joints in a lap joint configuration through varying the aforementioned dimensional process parameters. T. Solenbach made basic electrical model calculations using simple resistance network methods for different weld seam layouts and concluded that by properly choosing the weld seam layout, the contact resistance could strongly be reduced [16]. The group of P.A. Schmidt observed that using curved weld beads instead of straight ones significantly increased the appearance of cold cracks and other weld defects during weld formation. Based on their results it can be derived that the use of curved welds is not appealing for battery joining applications. This research group also pointed out that weld contours consisting of 2 or 3 lines had significantly higher electrical conductivities, in their view stemming from the more uniform current flux distribution. Along these lines this weld geometry seems to be particularly promising for optimization. In unison with Solenbach's team, they also concluded that applying different weld seam layouts highly influenced the conductivity of electrical connections, but they also added that further investigations were necessary for a better understanding [17]. Ultimately, S. Hollatz's research group recently did an extensive study on this subject as well, although less systematically. Like T. Solenbach's group, they made simple resistance network approximations followed by numerical current density simulations for both single and double welds.

In order to support their simulation data, they also conducted experiments for both similar and dissimilar joint cases with a few selected weld bead layouts. Their most forward looking discovery was the description of a so-called edge current phenomenon. The core of which is that the current density along the edges of the overlap was significantly higher as compared to the inner contact area [18].

It was shown that several works focus on weld bead layout optimization processes for laser welding applications in a lap joint configuration [16–18]. However, the majority of the existing papers focus on the numerical simulation of this subject. Consequently, there is a lack of systematic experimental investigations in this field. Hence, to make the picture more complete, simultaneous investigation of the effect of the weld seam layouts on both mechanical and electrical properties is carried out within this study. Along these lines, based on a systematic experimental study, in this paper we discuss the experimental results of a number of joint optimization possibilities related to the weld seam layout both in terms of electrical and mechanical considerations. The discussed aspects can be optimized both individually and simultaneously, as well. Our ultimate goal is to identify conditions that result in minimal electrical resistance and maximum mechanical strength, while keeping the laser related process parameters (such as laser power, scanning speed, underfocusing, and weld length) constant.

2 Experimental

A custom-designed laser welding station, created by Indupro Ltd. (<https://indupro.hu/>), was used to create specimens that were laser welded in the lap geometry. The welding station includes a custom sample holder jig, that is, schematically shown in Fig. 1, positioned underneath the laser beam.

The energy source for welding was a Yb-doped, single mode, continuous wave fiber laser (Trumpf TruFiber 1000: 1075 nm wavelength, 1000 W maximum power, unpolarized beam, $M^2 = 1.2$). The beam was focused onto

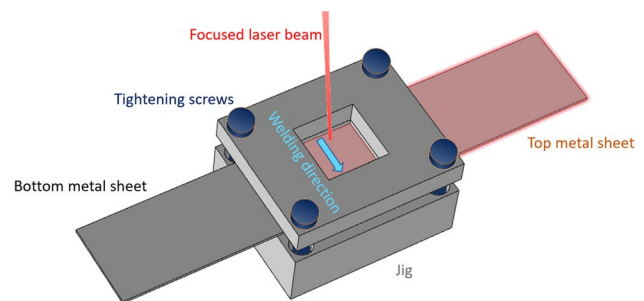


Fig. 1 The illustration of the experimental welding jig used for fixing the two metal sheets to be joined

a 0.61 mm diameter spot ($1/e^2$) using the 264 mm focal length field lens of a programmable focusing optic device (Trumpf PFO20-2). The top surface of the metal sheets to be welded was parallel to the beam waist. The samples were two pieces of cold-rolled, rectangular-shaped DC01 steel sheets, each having a thickness of 0.5 mm and a width of 16 mm. They were held together in a tailor-made jig with a fixed overlap length of 16 mm. Four screws, situated at the corners of the jig, were used to hold the upper portion of the jig in place, as shown in Fig. 1, and exert a fairly uniform compression of the steel sheets. The scanning speed was adjustable from 1 to 1100 mm/s.

The use of the scanner optic unit in the laser welding system was pivotal since the experiments conducted in this study focused on investigating the effect of the different weld bead configurations within the 10×10 -mm-sized rectangular window of the jig, defining the overlapping zone.

Based on the presumption that the base material of a typical Li-ion cell case (most frequently nickel coated steel or Hilumin™) possess rather similar mechanical, electrical, and chemical properties to DC01 steel, the latter cold rolled, low carbon content, non-alloy steel was chosen as model material for this study.

For our studies, we produced autogenous welds in lap joint geometry to replicate the frequently used stripe bonding procedures, as well as the direct bus-bar-to-battery-cap junctions. When welding batteries or cells in large quantities, notably in the automotive industry, this joint geometry is often regarded as the best, if not the only, joining option [19–21].

During our present investigation we were focusing on laser welded joint property (electrical and mechanical) optimization through configuring the layout of the weld beads in the overlapping zone. Thus, we chose a fixed set of laser processing parameters (based on our previous works) that can yield a highly stable and well reproducible weld bead. As a result, we kept the incoming laser at 400 W constant power and the scanning speed at 50 mm/s value. [22] Along these lines all other process parameters, such as the welding atmosphere's pressure and its composition, the temperature of the ambient air, and the incidence angle of the laser beam with respect to the surface normal were also kept unchanged throughout the experiments. These conditions were 23 °C ambient temperature, 0° laser incidence angle, and atmospheric air atmosphere.

Among the aforementioned conditions, full penetration welds were produced, as demonstrated on the cross-sectional macrograph shown in Fig. 2.

Please note that the macrograph shown in Fig. 2 was taken on a fractured sample, but is still convincingly demonstrate that the weld fully penetrates the total thickness of the two overlapping metal sheets.

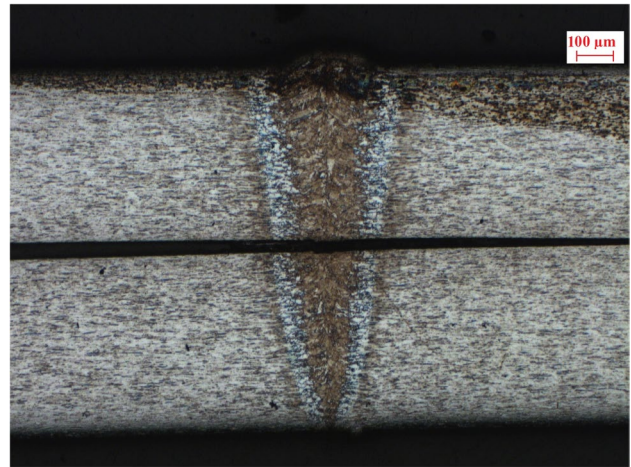


Fig. 2 Cross-sectional optical macrograph of a laser generated weld (400 W laser power, 50 mm/s scanning speed)

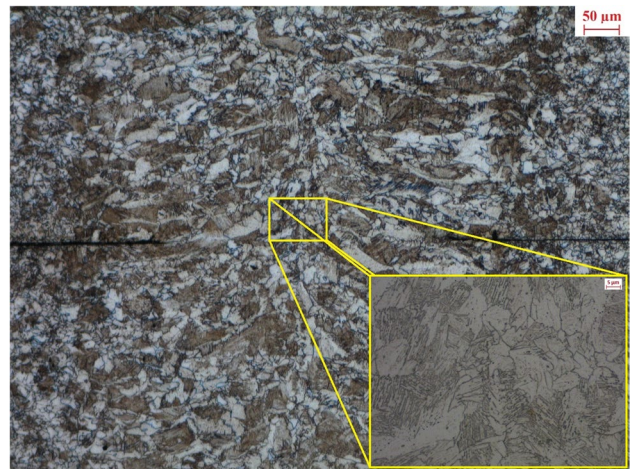


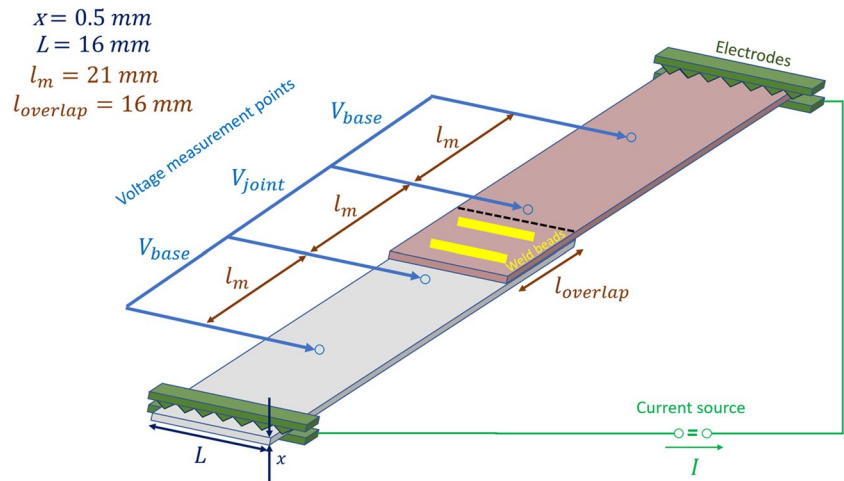
Fig. 3 Cross-sectional optical macrograph of the weld seam (400 W laser power, 50 mm/s scanning speed) taken at the interface of the two metal sheets at $\times 100$ magnification and on an inner area at $\times 1000$ magnification (inset)

To demonstrate the quality of the joints in Fig. 3, a cross-sectional optical macrograph is presented, taken of the weld seam at the interface of the two metal sheets after polishing and etching. On the inset another image acquired at $\times 10$ higher magnification over the central part of the same area (in the central region of the seam) reveals the grain structure of the resolidified metal.

It is evident that no cracks or voids are present within the body of the weld seam near the sheet interface. The seam has a highly regular and uniform grain formation.

To better visualize the experimental setup, a welded specimen is schematically depicted in Fig. 4 along with the critical dimensions and the configuration/arrangement of the probes of the 4-point probe measurement.

Fig. 4 Schematic view of the laser welded specimen and the arrangement of probes for the 4-point probe resistance measurement



Only very recently do manufacturers and research groups feel the need for a complete assessment of the electrical characteristics of the laser welded joints. As a result, the electrical conductivity of a joint cannot be measured using a standardized method yet. As a substitute the measurement technique developed by Schmidt et al. is adopted by research groups working on battery welding [16, 23, 24]. Here, the so-called k factor is calculated using three voltage drops, namely V_{joint} , V_{base1} , and V_{base2} measured over equal sample lengths (l_m), which shows how closely the bonding resistance relates to the base resistances of the sheets to be welded [17]. When the two sheets to be welded are made of the same material, V_{base1} and V_{base2} become identical and can be replaced by V_{base} (see Fig. 4), which simplifies the computation of the k factor and yields.

$$k = \frac{V_{joint}}{V_{base}} = \frac{R_{joint}}{R_{base}}. \quad (1)$$

By employing a fixed, 21 mm length 4-point-probe voltage measurement method, we determined the electrical resistance of both the welded and non-welded regions of the metal specimens. Before putting the electrical measurement probes on the sample surfaces, both surfaces were cleaned with acetone. In order to ensure homogeneous electric current flow along the samples electrodes were fastened to the two edges of the samples that covered the entire width of the sheets. Current was supplied by a DC power supply unit (TTi CPX200, with an accuracy of 1.1% for the maximum current of 10 A employed during the measurement process). A desktop multimeter (Keithley 2401, with a measurement accuracy of 0.1% in the voltage range used for our investigations) was employed to measure the V_{joint} , V_{base} voltages. In order to prevent the Joule heat of the measuring currents from significantly changing the temperature and hence the electrical resistance of the sample, the measurement procedure was carried out in the

shortest time that was technically feasible (typically within 0.5–1.0 s).

We quantified the mechanical strength of the laser welded specimens by measuring the maximum tensile-shear force between the laser welded metal sheets using a mechanical tester (Tinius Olsen H5KT, 0.1% measurement accuracy in the force range of our study). We note that during the tensile testing the fracture occurred always at the interface of the two neighboring metal sheets within the weld seam, regardless of the weld seam layout used. After fracturing the joints, optical microscope images of the two facing surfaces of DC01 sheets were acquired with an Olympus DSX510 3D optical microscope and used to determine the cross section of the weld. Using an image processing software (ImageJ), the digital 2D and 3D microscope pictures captured were examined [25]. The joint's cross section was independently measured on the two facing surfaces of the metal sheets. We found that the cross-sectional values measured on the two facing surfaces varied by less than 1%. The maximum tensile-shear force value was divided by the average of the two cross sectional areas to determine the tensile-shear strength value of the joint.

3 Results and discussion

In our experiments reported here, we focused on changing several dimensional welding conditions during the joining procedure while keeping the laser parameters constant. During the experiments, the laser power was kept at a constant 400 W, the welding speed was fixed at 50 mm/s and the laser spot diameter was also fixed at a value of 0.61 mm ($1/e^2$). These parameters were chosen according to our previous results [22], since this set of process parameters yielded rather consistent, so called single wave type weld bead morphology with highly reproducible properties and stable weld area values.

In every experimental series presented, strictly straight welds were used. This was important on one hand to keep the number of variables more manageable and on the other hand to circumvent the appearance of weld defect such as cold cracking based on the observations of P.A. Schmidt's group as previously mentioned [17].

The electrical resistance and the maximal force that a joint can withstand without fracture are highly dependent on both the size of the weld area and its shape [26, 27]. The weld area size (when the laser parameters are kept constant) is defined by the number of segments and the segment length used in a particular weld seam layout. The shape is much more complex as it considers the orientation and spacing of the segments, as well.

Consequently, two immediate possibilities arise for optimizing the weld seam layout for improving the electrical and mechanical joint properties:

- Optimizing the shape of the welds
- Changing the size of the welds

3.1 The effect of the shape of the welds on the electrical and mechanical properties

Laser welding of metal sheets in a lap joint configuration usually consists of a single, straight line or a circle symmetrically placed in the center of the overlapping zone. However, a given bead length can be realized in a plethora of other possible combinations of segments. In order to make the investigation more manageable, we investigated straight lines with symmetrical shape configurations only, meaning the bead or beads were always centrally symmetrical and were placed in the geometrical center of the overlapping

zone. The overlap between the two metal sheets was also fixed at 16 mm during these investigations.

When investigating the effects of the weld area shape the size of the weld areas were kept constant: the average weld area size of an 8 mm long segment prepared with the laser process parameters defined in the experimental part was $(2.62 \pm 0.05) \text{ mm}^2$. The individual values can be seen in Fig. 5 with the average being indicated by the horizontal dark blue line. The two light blue lines represent the absolute error at 95% confidence level. Each bar represents the data of 3 independent measurements.

For the present study, 7 different weld bead shapes were defined, realized and characterized in terms of electrical and mechanical properties. The results are summarized in Fig. 6. The photographs indicate the bead contour and the contour's relative position to the longer edge of the stripes (and the measuring electrical current). As an example, the symbol “/” means a single straight bead parallel to the measuring current and tensile force and a “=” symbol means a double bead perpendicular to it.

We plotted the k factor of each bead shape against their mechanical strength to make tendencies visually easier to identify. In the chosen representation the best welds, in terms of both electrical and mechanical properties, can be found in the lower right quadrant of Fig. 6.

It can be noted that those contours that contain two non-overlapping, parallel sections (with respect to each other) possess greater mechanical strength, although their total length is identical to single section shapes. It is also interesting to note that when rotating the single perpendicular bead by 90° the average mechanical strength rises from (419.1 ± 8.5) to (452.0 ± 48.4) MPa. This is in line with the expectations as a parallel section is affected by higher torque during the mechanical tests. Therefore, samples with

Fig. 5 The measured weld areas of the different weld bead shapes

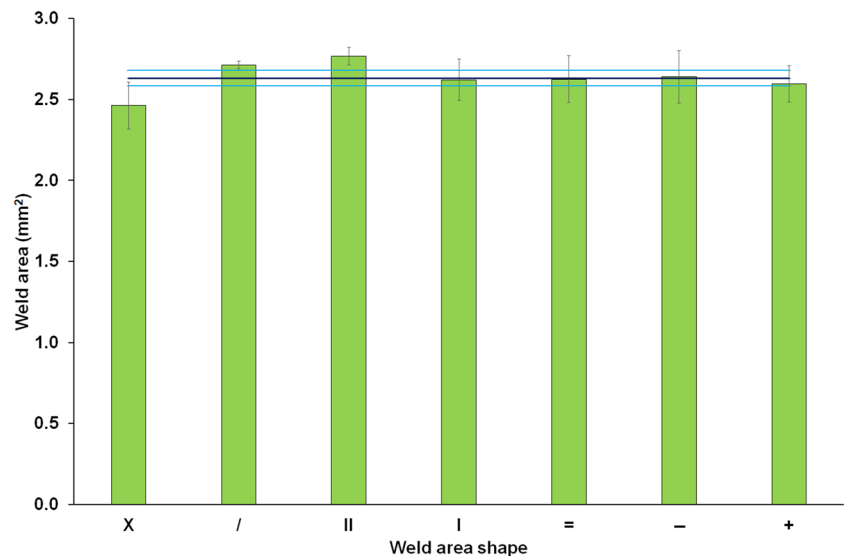
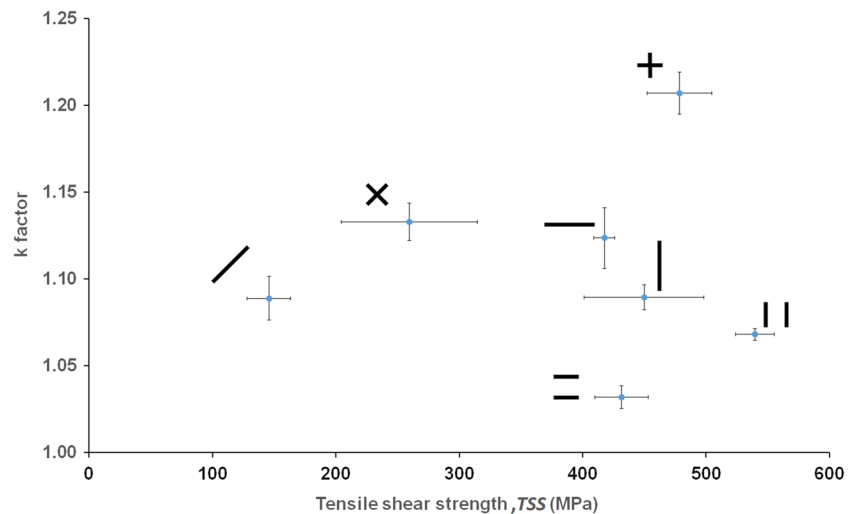


Fig. 6 The k factor and the tensile shear strength of the differently shaped welds with constant weld area. (The error bars represent absolute error at 95% confidence level. Each point represents the data of 3 independent measurements.)



the double parallel shape exhibit the highest mechanical strength, namely (540.3 ± 15.6) MPa.

In terms of electrical measurements using a double perpendicular configuration seems to be the best with a k factor of 1.031 ± 0.006 value. In general, weld shapes that include two non-overlapping sections yield better electrical and, in some cases, better mechanical properties than single segment contours. For instance, when using double welds instead of single one the k factor decreases from 1.089 ± 0.007 to 1.067 ± 0.003 in the parallel case and from 1.123 ± 0.017 to 1.031 ± 0.006 in the perpendicular one.

When considering beads oriented at a 45° angle, they seem to possess worse electrical and mechanical properties when compared to the parallel and perpendicular orientations. Using an overlapping double configuration of this contour, the “x” shape improves the mechanical properties, but decreases the conductive capabilities. When rotating this “x” shape and forming a “+” the mechanical strength rises even higher, but the k factor rises considerably. We also note that at this 2.62 mm^2 weld area size the electrical properties of the base metal could not be surpassed (meaning the k factor could not be reduced under 1) regardless of the weld bead shape.

According to these experiments, weld bead shapes consisting of multiple non-contacting segments behave significantly better both in terms of electrical and mechanical properties and should be preferable.

3.1.1 Multiple parallel welds

Based on the observations of the previous section we paid extra attention towards making multiple welds (i.e., those consisting of multiple parallel, nonoverlapping segments) and examined their electrical and mechanical behavior.

For these experiments, we chose the shape that exhibited the best electrical property, namely the one in which the weld beads were oriented perpendicular to the direction of

the test current (or equivalently along the longer edge of the sheets). Here also, keeping the total weld area constant was essential. To investigate the effect of the distance between the individual segments, we divided the total 16 mm bead length up to a maximum of 6 equal length segments (each one is about 2.7 mm) and varied the spacing between them and report below the electrical behavior of these bead structures. A schematic figure describing the terminology and the relationship between the individual parameters of the parallel structures is presented in Fig. 7.

The results of the electrical measurements for multiple weld configurations are summarized in Fig. 8.

We note that the difference in the maximum spacing value for each series results from the constraint that the overlapping zone size of the metal sheets was fixed at 16 mm ($E \leq 8$ mm for each series). Please note that for these measurement series we did not make samples with sub-1 mm spacing to avoid any possible weld bead overlap.

One can immediately note that for each set the increase of the spacing, s between consecutive segments resulted in a decrease in the k factor, an effect that becomes more significant with the increase of the number of segments. As an example, when using a pattern consisting of two 8 mm long beads and increasing the distance between the 2 parts from 1 to 8 mm, the k factor falls from 1.056 ± 0.016 to 0.866 ± 0.012 that is more than a 20% relative drop!

As described in the Introduction section, Hollatz et al.’s electrical simulations show that the electrical current flows dominantly through the frontal and rear edges of the weld area. In our case, this translates to the two outermost weld segments being dominant in the electrical conduction and the inner bead segment(s) contribution being negligible. Consequently, this spacing representation can be converted into a graph where the prime parameter is the distance between the two outermost segments, i.e., the weld bead group’s “extent,” denoted as E (cf. Figure 5). This representation is shown in Fig. 9.

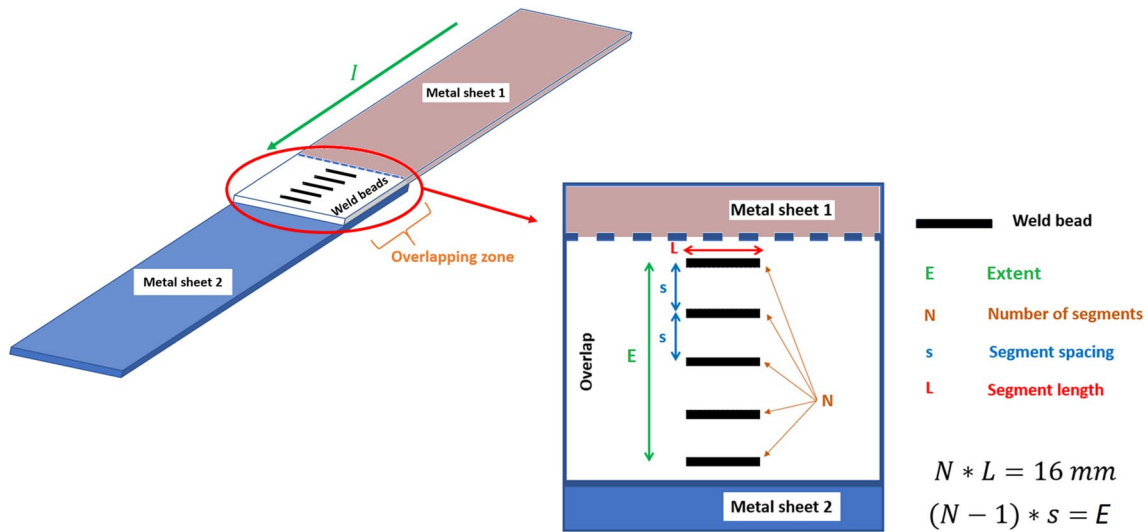
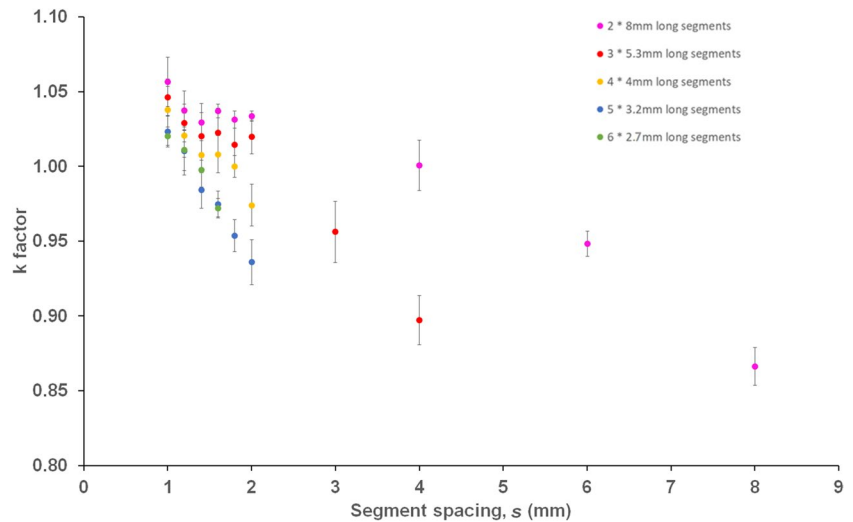


Fig. 7 The terminology of multiple welds (the white areas indicate the overlapping zone between the two metal sheets)

Fig. 8 The k factor of multiple welds with different spacing. Each set represents a series of different segment lengths. (The error bars represent absolute error at 95% confidence level. Each point represents the data of 3 independent measurements.)



From Fig. 9, it is evident that for any given segment length, increasing the distance between the outermost segments yields a significant decrease in k factors. However, in this representation, it is also clear that the length of these outermost segments is also a significant factor. As an example, when the extent is 8 mm and shortening the segment lengths from 8 mm down to 2.6 mm, the k factor gradually increases from 0.866 ± 0.012 up to 0.971 ± 0.013 in value, that is, over a 10% increase. The same phenomenon can also be observed at smaller extent values as well, albeit the change in electrical properties is much less significant.

In terms of mechanical shear strength, the results only showed a clear tendency when being plotted against the extent of the welds. This is shown in Fig. 10.

These results are in line with the behaviors observed at the weld bead shape investigations, namely that the greater

the extent of the weld bead in the direction of the testing force the greater the measured strength. This phenomenon stems from the testing method as the bead structures with larger extents are more resilient against the twisting torque that arises during testing.

It is also interesting to analyze the intercept of the resulting graph. The extreme case of zero extent can be interpreted as if the two outermost seams of the structures overlap thus forming a single weld bead in the middle of the overlapping zone. Along these lines, the two weld areas overlap as well, and as a result, the total weld area of the weld beads becomes half of the original value resulting in a strength of $2 \times 186.81 \text{ MPa} = 373.6 \text{ MPa}$, that is, rather close to the value reported previously for single perpendicular weld beads, namely $(419.1 \pm 8.5) \text{ MPa}$.

Fig. 9 The k factor of multiple welds with different extent. Each set represents a series of different segment lengths. (The error bars represent absolute error at 95% confidence level. Each point represents the data of 3 independent measurements.)

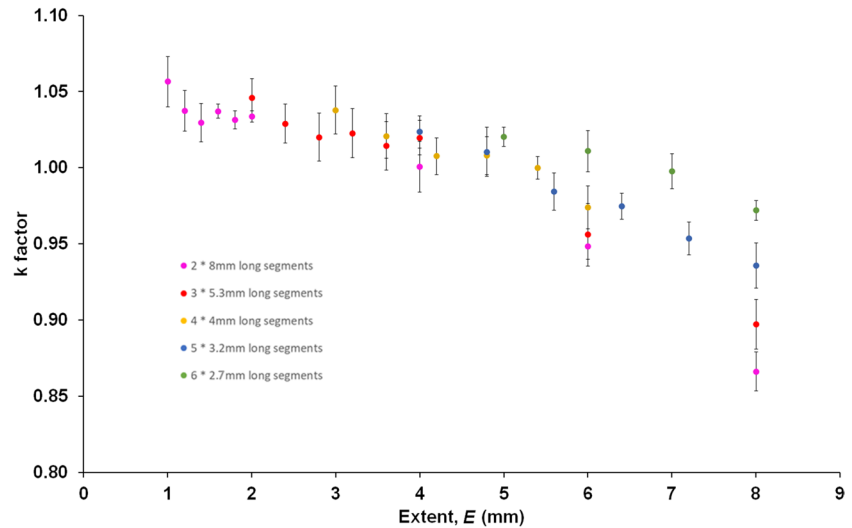
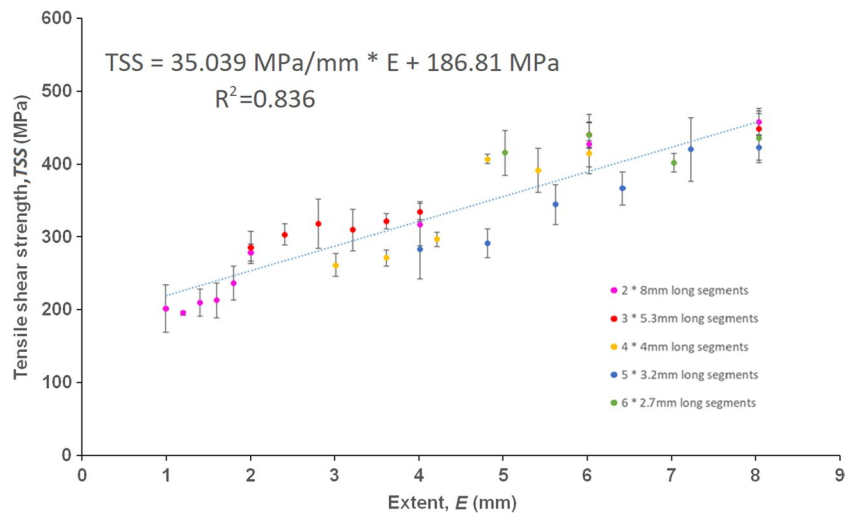


Fig. 10 The tensile shear strengths of multiple welds with different extent. (The error bars represent the absolute error at 95% confidence level. Each point represents the data of 3 independent measurements.)



3.2 The effect of the weld area size on the electrical and mechanical properties

As previously mentioned, besides optimizing the weld area shape, another dimensional parameter that allows for joint property improvement is the size of the weld area between the two metal sheets.

One can increase the weld area by two means:

- Increasing the length of a segment, or
- Increasing the number of segments

The two methods can of course be applied simultaneously, as well.

The two ways will be discussed separately in the following sections, while ensuring that the previously discussed extent (E) was kept at a constant 10 mm value to mitigate the possible effects of weld shape changes.

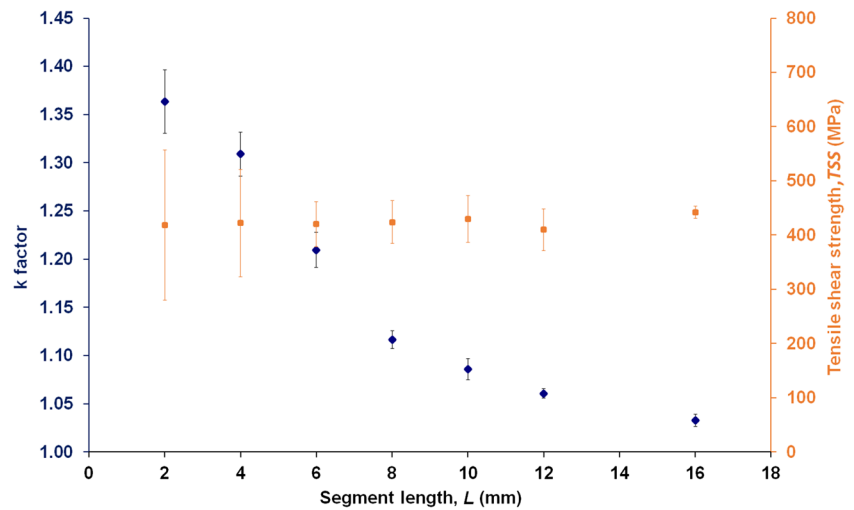
3.2.1 The effect of the segment length

For these experiments single segment welds were produced with different segment lengths, all situated centrally or symmetrically within the width of the metal stripes.

The results obtained from the electrical and mechanical measurements are shown in Fig. 11. The segment length was varied in 2 mm steps from 2 to 16 mm, the latter corresponding to the case when the two metal stripes were joined across the entire width.

According to these results with increasing single segment length, the k factor converges to the value of ($k=$)1. It is also interesting to note that for bead length beyond 8 mm (the half width of the sample) the rate of decrease of the k factor slows down. With increasing segment length, the error of the measurement points decreases steadily. We assume that the larger error bars at short weld lengths originate from the fact that at shorter laser irradiation times, the stability

Fig. 11 The k factor (blue symbols) and tensile shear strength (orange symbols) values for various single segment lengths. (The error bars represent absolute error at 95% confidence level. Each point represents the data of 3 independent measurements.)



of our laser welding station becomes limited; therefore, the effect of instabilities is more expressed on the shorter segments. Moreover, as described by both W. R. Harp and J. Tu continuous wave fiber lasers usually exhibit initial transient power instability during emission in the first few μ s of the power on phase when used in a short pulse mode [28, 29]. This effect can be more dominant during an overall shorter processing time (the processing time of a 2 mm long segment with 50 mm/s scanning speed is 40 ms).

In terms of mechanical properties, it can be said that the strength of the samples was not affected by the weld bead length and remained constant around the average of (427 ± 10.1) MPa. We also note here that the higher error bars of relatively short welds possibly originate from the fact that the area determination error yields a larger relative error for shorter seam sizes during the manual microscope image analysis.

3.2.2 The effect of the number of segments

Another way to increase the weld area size, aside from increasing the length of segments, is to increase their number. For this investigation segment structures of constant length ($L=8$ mm) and extent ($E=10$ mm) was made in which each segment was oriented perpendicular to test current (i.e., along the shorter, 16 mm width of the metal stripes) and in the geometrical center of the overlapping zone. When the number of segments was varied in $2 \leq N \leq 11$ range, the spacing of the segments was gradually changed from 10 to 1 mm.

During our experiments, we paid careful attention to ensure that the weld area depends linearly on the number of segments, a condition that holds in this set within 1% error. In other words, samples with 4 segments have a weld area 4 times as large as a sample with a single bead.

The results of the electrical and mechanical measurements are shown in Fig. 12.

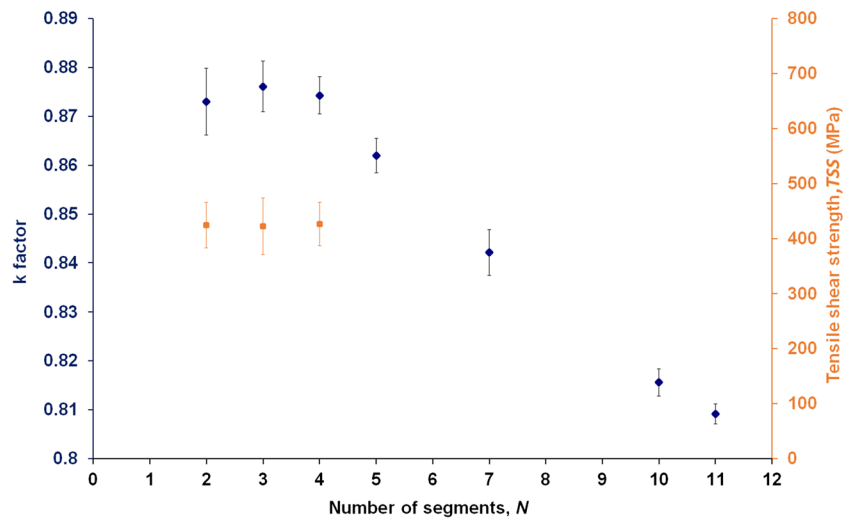
It is an interesting thing to note that increasing the number of welds beyond two does not result in a significant decrease in k factor. This is caused by the phenomenon discussed by Hollatz et al. [18]. According to their numerical equivalent circuit modelling calculations, most of the electric current flows through the frontal and rear edges (practically the first and the last segment) of the welded area when two or more weld beads are present. This explains why the k factor of samples with relatively small number of seams ($N=2, 3,$ and 4) is identical to each other within error. Our results show that when increasing the number of segments by a factor of ten, the k factor can decrease slightly. This indicates that perceptible current starts to flow through the inner segments that are further away from the edges, as they start to participate in the electrical conduction process. However, the magnitude of this decrease reflects that this effect is minor, and the slight benefit might not be sufficient when considering the extra manufacturing effort required to achieve it.

The mechanical testing of these samples was limited since welded joints having a weld area above a critical value could withstand more force (above 5000 N) than the materials' strength of the base metal of our stripes, i.e., failure of the laser welded samples will occur inside the base metal and not in the weld area. Consequently, we could only test the strength of the joint up until $N=4$. For those specimens where the measurement process could be conducted it was clear that the tensile shear strength of the joints was not dependent on the weld multiplicity, as the results scattered around (424 ± 21) MPa strength in every case.

3.3 The comparison of the effects of different dimensional optimization aspects

In Table 1, we summarized the gains achieved of the different optimization approaches both in terms of electrical

Fig. 12 The *k* factor (blue symbols) and tensile shear strength (orange symbols) values of samples with different number of segments of equal length (*L* = 8 mm) and constant extent (*E* = 10 mm). (The error bars represent absolute error at 95% confidence level. Each point represents the data of 3 independent measurements.)



and mechanical properties. The gain is defined according to the following equation:

$$\text{Gain} = \frac{\text{Best value} - \text{Worst value}}{\text{Worst value}} \quad (2)$$

Naturally, in case of electrical properties, the lower *k* factors represent the more favorable conditions; as a result, the “gains” here as to the definition are negative as indicated by the “-” signs in Table 1.

It is important to note that each aspect was investigated in separate sets, i.e., when every other parameter and condition was kept constant.

In Table 1, the extent (*E*), segment number (*N*), spacing (*s*), and segment length (*L*) values belonging to the samples

with the “best” and “worst” electrical or mechanical properties are also given.

According to our results, the shape of the weld has a huge impact on the mechanical strength of the lap welded samples. This is evidenced by the results that the tensile shear strength is increased by almost 3-folds when comparing the best and worst patterns. Moreover, the shape has a rather significant role on the electrical properties, as well. We also reported results that among the general shapes, weld configurations consisting of multiple straight segments have a significant impact on the electrical and mechanical property optimization processes. Within the parameter range studied, the best and worst multiple weld configurations showed a 136% and 18% relative improvement in terms of mechanical

Table 1 The *k* factor and tensile shear strength gains of the different optimization processes

		Shape of the welds				Area of the welds			
		General shapes		Optimizing double configurations		Segment length		Number of segments	
<i>k</i> factor	Best	1.031±0.006		0.866±0.012		1.032±0.006		0.809±0.002	
			<i>E</i> (mm) 8 <i>N</i> 2 <i>s</i> (mm) 8 <i>L</i> (mm) 8			<i>E</i> (mm) - <i>N</i> 1 <i>s</i> (mm) - <i>L</i> (mm) 16		<i>E</i> (mm) 10 <i>N</i> 11 <i>s</i> (mm) 1 <i>L</i> (mm) 8	
	Worst	1.207±0.012		1.056±0.016		1.363±0.033		0.876±0.005	
			<i>E</i> (mm) 1 <i>N</i> 2 <i>s</i> (mm) 1 <i>L</i> (mm) 8			<i>E</i> (mm) - <i>N</i> 1 <i>s</i> (mm) - <i>L</i> (mm) 2		<i>E</i> (mm) 10 <i>N</i> 3 <i>s</i> (mm) 5 <i>L</i> (mm) 8	
	Gain	-15%		-18%		-24%		-8%	
Tensile shear strength (MPa)	Best	539.6±15.6		466.9±19.1		442±11.15		426±41.5	
			<i>E</i> (mm) 8 <i>N</i> 2 <i>s</i> (mm) 8 <i>L</i> (mm) 8			<i>E</i> (mm) - <i>N</i> 1 <i>s</i> (mm) - <i>L</i> (mm) 16		<i>E</i> (mm) 10 <i>N</i> 4 <i>s</i> (mm) 3.3 <i>L</i> (mm) 8	
	Worst	145.7±17.5		197.1±1.7		410±38.5		422±51.9	
			<i>E</i> (mm) 1.2 <i>N</i> 2 <i>s</i> (mm) 1.2 <i>L</i> (mm) 8			<i>E</i> (mm) - <i>N</i> 1 <i>s</i> (mm) - <i>L</i> (mm) 12		<i>E</i> (mm) 10 <i>N</i> 3 <i>s</i> (mm) 5 <i>L</i> (mm) 8	
	Gain	+270%		+136%		+8%		NA	

and electrical properties, respectively. When considering the effect of the area of the welds on the aforementioned properties, we can say that they have little to no effect on the tensile shear strength values, while the size of the weld area has a considerable effect on the electrical property. For instance, the shortest and longest investigated single beads had an absolute difference exceeding 20%.

4 Conclusion

In this paper, we described how several dimensional process parameters affect the electrical and mechanical properties of the laser welded joint.

Our results show that when performing dimensional optimization on laser welded DC01 steel stripes, the following tendencies should be expected:

- From especially the electrical standpoint, it is highly beneficial to use a weld layout that is made up of at least two non-overlapping segments.
- For better electrical properties, the bead should include mostly perpendicular segments, while for better mechanical properties segments oriented parallel to the direction of the current flow are preferred.
- For achieving better electrical and mechanical properties in general the individual segments should be as long as practically feasible.
- Larger distance between the individual weld bead segments is favorable both in terms of electrical and mechanical properties.

Finally, these dimensional tendencies—when applied jointly—may add up synergistically, offering grounds for further joint improvements in the mechanical and electrical properties of the laser welded structures.

Despite our remarkable results, further experimental investigation is necessary in the future. One aspect to tackle is study weld seam layouts that involve curved lines. Extending the scope of the investigation to highly conductive materials and to the laser welding of dissimilar metals is also an important future goal.

Acknowledgements We would like to thank the staff of the Department of Mechanical Engineering and Material Sciences of the University of Dunaújváros for helping with the preparation and analysis of the cross-section macrographs of the laser welded samples.

Author contribution All authors contributed to the study conception and design. Material preparation, data collection, and analysis were performed by GH and AK. TSz and ZsG supervised the entire work. The first draft of the manuscript was written by GH and all authors contributed to the improvement of the manuscript. All authors read and approved the final manuscript.

Funding Open access funding provided by University of Szeged. This work was supported by the Hungarian EFOP-3.6.1–16-2016–00014 project, entitled “Research and development of disruptive technologies in the area of e-mobility and their integration into the engineering education.”

Declarations

Competing interests The authors declare no competing interests.

Open Access This article is licensed under a Creative Commons Attribution 4.0 International License, which permits use, sharing, adaptation, distribution and reproduction in any medium or format, as long as you give appropriate credit to the original author(s) and the source, provide a link to the Creative Commons licence, and indicate if changes were made. The images or other third party material in this article are included in the article’s Creative Commons licence, unless indicated otherwise in a credit line to the material. If material is not included in the article’s Creative Commons licence and your intended use is not permitted by statutory regulation or exceeds the permitted use, you will need to obtain permission directly from the copyright holder. To view a copy of this licence, visit <http://creativecommons.org/licenses/by/4.0/>.

References

1. Lee SS, Kim TH, Hu SJ, Cai WW, Abell JA (2010) Joining technologies for automotive lithium-ion battery manufacturing: a review. ASME 2010 International Manufacturing Science and Engineering Conference, Volume 1. Erie, Pennsylvania, USA. October 12–15, 2010. pp. 541–549. <https://doi.org/10.1115/MSEC2010-34168>
2. Ready JF (2001) LIA handbook of laser materials processing, Magnolia Publishing, Orlando, USA, ISBN: 978-3-540-41770-5
3. Ferjutz K, Davis JR (1993) Welding, brazing and soldering. In: ASM handbook, vol 6. ASM International. <https://doi.org/10.31399/asm.hb.v06.9781627081733>
4. Cao X, Wallace W, Immarigeon JP, Poon C (2007) Research and progress in laser welding of wrought aluminum alloys. II. metallurgical microstructures, defects, and mechanical properties. Mater Manuf Process. 18(1):23–49. <https://doi.org/10.1081/AMP-120017587>
5. Yan J, Gao M, Zeng X (2010) Study on microstructure and mechanical properties of 304 stainless steel joints by TIG, laser and laser-TIG hybrid welding. Opt Lasers Eng 48(4):512–517. <https://doi.org/10.1016/j.optlaseng.2009.08.009>
6. Xia M, Tian Z, Zhao L, Zhou YN (2008) Metallurgical and mechanical properties of fusion zones of TRIP steels in laser welding. ISIJ Int 48(4):483–488. <https://doi.org/10.2355/isijinternational.48.483>
7. Heydari H, Akbari M (2020) Investigating the effect of process parameters on the temperature field and mechanical properties in pulsed laser welding of Ti6Al4V alloy sheet using response surface methodology. Infrared Phys Technol 106:103267. <https://doi.org/10.1016/j.infrared.2020.103267>
8. Reisgen U, Olschok S, Holtum N (2019) Influencing the electrical properties of laser beam vacuum-welded Cu-Al mixed joints. J Laser Appl 31(2):022406. <https://doi.org/10.2351/1.5096093>
9. Trinh LN, Lee D (2020) The characteristics of laser welding of a thin aluminum tab and steel battery case for lithium-ion battery. Metals 10(6):842. <https://doi.org/10.3390/met10060842>

10. Brand MJ, Schmidt PA, Zaeh MF, Jossen A (2015) Welding techniques for battery cells and resulting electrical contact resistances. *J Energy Storage* 1:7–14. <https://doi.org/10.1016/j.est.2015.04.001>
11. Li Z, Rostam K, Panjehpour A, Akbari M, Karimipour A, Rostami S (2020) Experimental and numerical study of temperature field and molten pool dimensions in dissimilar thickness laser welding of Ti6Al4V alloy. *J Manuf Process* 49:438–446. <https://doi.org/10.1016/j.jmapro.2019.11.024>
12. Jiang D, Alsagri AS, Akbari M, Afrand M, Alrobaian AA (2019) Numerical and experimental studies on the effect of varied beam diameter, average power and pulse energy in Nd: YAG laser welding of Ti6Al4V. *Infrared Phys Technol* 101:180–188. <https://doi.org/10.1016/j.infrared.2019.06.006>
13. Tsai Y, Lo Y, Raza MM, Saleh AN, Chuang T, Chen C, Chiu C (2023) Optimization of lap-joint laser welding parameters using high-fidelity simulations and machine learning mode. *J Mater Res Technol* 24:6876–6892. <https://doi.org/10.1016/j.jmrt.2023.04.256>
14. Sun C, Dehkordi MHR, Kholoud MJ, Azimy H, Li Z (2023) Systematic evaluation of pulsed laser parameters effect on temperature distribution in dissimilar laser welding: a numerical simulation and artificial neural network. *Opt Laser Technol* 163. <https://doi.org/10.1016/j.optlastec.2023.109407>
15. Maculotti G, Genta G, Galetto M (2023) Optimisation of laser welding of deep drawing steel for automotive applications by Machine Learning: a comparison of different techniques. *Qual Reliab Eng Int* 1–18. <https://doi.org/10.1002/qre.3377>
16. Solchenbach T, Plapper P, Cai W (2014) Electrical performance of laser braze-welded aluminum–copper interconnects. *J Manuf Process* 16:183–189. <https://doi.org/10.1016/j.jmapro.2013.12.002>
17. Schmidt PA, Schweier M, Zaeh MF (2012) Joining of lithium-ion batteries using laser beam welding: electrical losses of welded aluminum and copper joints. *ICALEO 2012 Paper #805*. <https://doi.org/10.2351/1.5062563>
18. Hollatz S, Kremer S, Ünübayir C, Sauer DU, Olowinsky A, Gillner A (2020) Electrical modelling and investigation of laser beam welded joints for lithium-ion batteries. *Batteries* 6(2):24. <https://doi.org/10.3390/batteries6020024>
19. Zhou MC (2016) *Advances in battery manufacturing, services, and management systems*. IEEE Press, Cambridge, England
20. Schmidt PA, Schmitz P, Zaeh MF (2016) Laser beam welding of electrical contacts for the application in stationary energy. *J Laser Appl* 28:022423. <https://doi.org/10.2351/1.4943908>
21. Mehlmann B, Gehlen E, Olowinsky A, Gillner A (2014) Laser micro welding for ribbon bonding. *Phys Proc* 56:776–781. <https://doi.org/10.1016/j.phpro.2014.08.085>
22. Horváth G, Körmöczi A, Szörényi T, Geretovszky Zs (2023) Bead morphology of laser welded steel sheets and its correlation to the joint's electrical and mechanical properties. *J Laser Appl* 35:022020. <https://doi.org/10.2351/7.0000996>
23. Dimatteo V, Ascari A, Fortunato A (2019) Continuous laser welding with spatial beam oscillation of dissimilar thin sheet materials (Al-Cu and Cu-Al): process optimization and characterization. *J Manuf Process* 44:158–165. <https://doi.org/10.1016/j.jmapro.2019.06.002>
24. Jarwitz M, Fetzer F, Weber R, Graf T (2018) Weld seam geometry and electrical resistance of laser-welded, aluminum-copper dissimilar joints produced with spatial beam oscillation. *Metals - Open Access Metall J* 8(7):510. <https://doi.org/10.3390/met8070510>
25. Schneider CA, Rasband WS, Eliceiri KW (2012) NIH image to ImageJ: 25 years of image analysis. *Nat Methods* 9(7):671–675. <https://doi.org/10.1038/nmeth.2089>
26. Yang YS, Lee SH (1999) A study on the joining strength of laser spot welding for automotive applications. *J Mater Process Technol* 94(2–3):151–156. [https://doi.org/10.1016/S0924-0136\(99\)00094-1](https://doi.org/10.1016/S0924-0136(99)00094-1)
27. Hamed M, Atashparva M (2017) A review of electrical contact resistance modeling in resistance spot welding. *Welding in the World* 61:269–290. <https://doi.org/10.1007/s40194-016-0419-4>
28. Harp WR, Dilwith JR, Tu JF (2008) Laser ablation using a long-pulsed, high-fluence, CW single-mode fiber laser. *J Mater Process Technol* 198:22–30. <https://doi.org/10.1016/j.jmatprotec.2007.06.062>
29. Tu J, Paleocrassas AG, Reeves N, Rajule N (2014) Experimental characterization of a micro-hole drilling process with short micro-second pulses by a CW single-mode fiber laser. *Opt Lasers Eng* 55:275–283. <https://doi.org/10.1016/j.optlaseng.2013.11.002>

Publisher's Note Springer Nature remains neutral with regard to jurisdictional claims in published maps and institutional affiliations.